RESEARCH ARTICLE

Metabolic Changes in Different Stages of Liver Fibrosis: *In vivo* Hyperpolarized ^{13}C MR Spectroscopy and Metabolic Imaging

Chung-Man Moon,[1,2] Sang-Soo Shin[2] Suk-Hee Heo,[2] Hyo-Soon Lim,[2] Myeong-Ju Moon,[3] Suchithra Poilil Surendran,[3] Ga-Eon Kim,[4] Il-Woo Park,[2] Yong-Yeon Jeong[2]

[1]*Quantitative Medical Imaging Section, National Institute of Biomedical Imaging and Bioengineering, National Institutes of Health, Bethesda, MD, USA*

[2]*Department of Radiology, Chonnam National University Hospital, Chonnam National University Medical School, 42 Jebong-ro, Dong-gu, Gwangju, 61469, South Korea*

[3]*Department of Radiology, Chonnam National University Hwasun Hospital, Hwasun, Republic of Korea*

[4]*Department of Pathology, Chonnam National University Hospital, Gwangju, Republic of Korea*

Abstract

Purpose: The objective was to assess metabolic changes in different stages of liver fibrosis using hyperpolarized C-13 magnetic resonance spectroscopy (MRS) and metabolic imaging.

Procedures: Mild and severe liver fibrosis were induced in C3H/HeN mice ($n = 14$) by injecting thioacetamide (TAA). Other C3H/HeN mice ($n = 7$) were injected with phosphate buffer saline (PBS) (7.4 pH) as normal controls. Hyperpolarized C-13 MRS was performed on the livers of the mice, which was accompanied by intravoxel incoherent motion (IVIM) diffusion-weighted imaging with 12 *b* values. The differential metabolite ratios, apparent diffusion coefficient values, and IVIM parameters among the three groups were analyzed by a one-way analysis of variance test.

Results: The ratios of [1-^{13}C]lactate/pyruvate, [1-^{13}C]lactate/total carbon (tC), [1-^{13}C]alanine/pyruvate, and [1-^{13}C] alanine/tC were significantly higher in both the mild and severe fibrosis groups than in the normal control group ($p < 0.05$). While the [1-^{13}C]lactate/pyruvate and [1-^{13}C]lactate/tC ratios were not significantly different between mild and severe fibrosis groups, the ratios of [1-^{13}C]alanine/pyruvate and [1-^{13}C]alanine/tC were significantly higher in the severe fibrosis group than in the mild fibrosis group ($p < 0.05$). In addition, D^* showed a significantly lower value in the severe fibrosis group than in the normal or mild fibrosis groups and negatively correlated with the levels of [1-^{13}C] lactate and [1-^{13}C]alanine.

Conclusions: Our findings suggest that it might be possible to differentiate mild from severe liver fibrosis using the cellular metabolic changes with hyperpolarized C-13 MRS and metabolic imaging.

Key words: Liver fibrosis, Hyperpolarized ^{13}C MRS, Metabolic imaging

Correspondence to: Sang-Soo Shin; *e-mail:* kjradsss@gmail.com

Introduction

Liver fibrosis in chronic liver disease can lead to cirrhosis, progressing ultimately to hepatocellular carcinoma [1]. Liver fibrogenesis is a dynamic interaction between cellular and molecular processes, which involves the accumulation of collagen, proteoglycans, and other macromolecules within the extracellular matrix [2]. Particularly, it is of interest to develop noninvasive techniques for the early diagnosis and characterization of fibrotic tissue since disease progression to liver cirrhosis can be prevented by early interventions with effective treatments. Although liver biopsy remains the gold standard technique of diagnosing and staging of liver fibrosis, this technique includes an invasive procedure with associated risk factors limiting its applicability to longitudinally monitor fibrosis progression or assessing therapeutic response [3].

Several imaging techniques have been developed for the diagnosis and staging of liver fibrosis. In general, ultrasound (US), x-ray computed tomography (CT), and magnetic resonance imaging (MRI) are used routinely to assess the morphologic alterations of cirrhosis, but they are limited for the evaluation of patients with earlier stages of liver disease [1, 4]. Although elastographic techniques implemented on US and MRI systems have gained the widest clinical acceptance in the context of liver fibrosis imaging, US elastography may be technically problematic in obese patients or those with ascites and a narrow intercostal space [5]. Meanwhile, the main limitation of MR elastography (MRE) is that liver stiffness may be affected by hepatic iron overload, steatosis, vascular congestion, cholestasis, and portal hypertension [5]. Moreover, detection of less advanced stages of fibrosis is still challenging [6].

Recently, liquid state hyperpolarized C-13 MR spectroscopy (MRS) has been recognized as a useful tool for the real-time investigation of cellular metabolism *in vivo* on a very short time scale [7]. According to hyperpolarized MR studies of the liver [7–10], pyruvate (Pyr) has been of main interest given its important role at the crossroad between oxidative phosphorylation and glycolysis. C-13 labeled substrates that have undergone dynamic nuclear polarization (DNP) produce C-13 signals with a 10,000-fold enhancement. Monitoring the enhanced signals during *in vivo* metabolic conversion of Pyr to alanine (Ala), lactate (Lac), and bicarbonate holds great promise for the improvement of tumor diagnosis and treatment monitoring, and assessment of cardiovascular pathologies, neurovascular and neurological diseases, and metabolic disorders [8]. Moreover, *in vivo* hyperpolarized C-13 MRS has broadened beyond detection of metabolic pathways associated with enzymatic reactions that were previously inaccessible through other imaging modalities [10]. To the best of our knowledge, although hyperpolarized C-13 MRS studies have been used to investigate changes of cellular metabolite on hepatic injuries [7–10], an *in vivo* hyperpolarized C-13 MRS study focusing on the staging of liver fibrosis for clinical translation has not been reported.

Thus, the purpose of this study was to investigate metabolic alterations in different stages of liver fibrosis using *in vivo* hyperpolarized C-13 MRS and metabolic imaging.

Materials and Methods

Animal Model

Six-week-old C3H/HeN mice (20–25 g) were obtained from Jung-Ang Lab Animal, Inc., Korea. Animal study was approved by the Chonnam National University Medical School Research Institutional Animal Care and Use Committee. Liver fibrosis in the C3H/HeN mice ($n = 14$) was induced by injections of thioacetamide (TAA) dissolved in phosphate buffer saline (PBS) three times per week *via* the intraperitoneal (IP) route. The mice were not anesthesized for the IP injections. The TAA concentration was adjusted by weight changes of the mice, which was incrementally varied by 10 mg from the starting concentration of 100 mg/kg [11]. Mice were allowed *ad libitum* per-oral access to 10 % ethanol-containing water along with TAA injection [11]. Ethanol intake was stopped 1 week before hyperpolarized C-13 MRS, and then mice were provided water sterilized by ultraviolet irradiation. In order to match the ages and weights in three groups, a severe fibrosis model was developed using C3H/HeN mice ($n = 7$) subjected to 15 weeks of prolonged TAA weight-adapted administration after baseline (6 weeks old), and a mild fibrosis model using C3H/HeN mice ($n = 7$) was injected with the TAA for 10 weeks after 5 weeks from baseline. Other C3H/HeN mice ($n = 7$) were injected with PBS (pH 7.4) as a control from baseline for 15 weeks.

Animal Preparation

The hyperpolarized [1-^{13}C] Pyr solution was administrated intravenously through the catheter inserted into the tail vein of mice. The breathing rate with a pressure transducer (Model 1025; SA Instruments Inc., Stony Brook, NY, USA) was monitored simultaneously during the acquisition of MRS and MRI data, maintaining at the range of 60–70 breaths per minute. In addition, core body temperature monitoring by a rectal temperature probe was maintained on temperature-controlled flowing water of approximately 36 °C.

Polarization and Hyperpolarized C-13 MRS

A volume of 25 µl of [1-^{13}C] pyruvic acid (Isotec, Miamisburg, OH) with 15 mM of an electron paramagnetic agent (trityl radical OX063; Oxford Instruments, Abingdon, UK) was hyperpolarized for ~1 h using the commercial Hypersense DNP polarizer (Oxford Instruments, Abingdon, UK) with 94.1 GHz microwaves in a

3.35 Tesla field at 1.4 K to an average polarization of 21 % (range 18.1–20.2 %) [7]. The hyperpolarized [1-^{13}C] Pyr was then rapidly dissolved in 4 ml of isotonic buffer containing 40 mM Trizma pre-set crystals (pH 7.6), 80 mM NaOH, 50 mM NaCl, and 2.69 mM disodium EDTA. The 80 mM hyperpolarized [1-^{13}C] Pyr solution was injected through the tail vein of the mouse which had been fasted for 12 h.

The pH was measured with an electronic balance (AUW-220D; Shimadzu, Tokyo, Japan) and ranged from 7.4 to 7.5. Hyperpolarized C-13 MRS studies were conducted on a 3 Tesla MR scanner (MR750; GE Healthcare, Milwaukee, WI, USA) with a dual-tuned H-1/C-13 linear volume transmit/ receive coil of 35 mm inner diameter (Rapid Biomedical, Würzburg, Germany). During the pre-scan period prior to acquiring C-13 spectra, linear shimming was performed over the liver parenchyma.

For the dynamic study, C-13 spectra were acquired every 2 s for 60 s simultaneously with the Pyr injection of 0.35 ml from a 5.5-mm slice included most of the liver. The spectra were acquired with a free induction decay chemical shift imaging (FIDCSI) pulse (5000 Hz acquisition bandwidth; 4096 points; a slice-selective radiofrequency pulse with a 10 ° flip angle). And then, C-13 two-dimensional (2D) spectroscopic metabolic images were acquired 25 s after the additional injection of 0.35 ml Pyr solution within 15 s after 1 h of hyperpolarization using the following parameters: field of view (FOV) of 50×50 mm^2 in a 5.5-mm axial slice through the liver, matrix size of 13×13, 256 spectral points (spectral resolution = 19.5 Hz), spectral width of 5000 Hz, and repetition time of 80 ms. The total time required to acquire a C-13 2D metabolic image was 14 s.

IVIM-DWI

After the hyperpolarized C-13 study, intravoxel incoherent motion (IVIM) diffusion-weighted imaging (DWI) with 12 b values (0, 10, 15, 20, 25, 30, 60, 75, 100, 200, 400, and 800 s/mm^2) was performed using a free-breathing single-shot echo-planar imaging (EPI) sequence, with the application of three diffusion gradient directions (TR/TE = 2500/71, slice thickness = 3 mm, FOV = 80×40 mm^2, matrix size = 92×92, and number of excitations = 16), and an acquisition time of 9 min and 42 s. Especially, our study used the alginate (3M ESPE, Seefeld, Germany)-water mixture to solve the problems such as air-tissue interface effects and motion artifacts, as previously described [10]. The solid alginate-mouse chamber was made after liquid alginate was poured around the mouse, with the head of the mouse to being outside the chamber for breathing.

Data Processing

Hyperpolarized C 13 MR spectra were analyzed using SAGE software (GE Healthcare), which were apodized by a 9-Hz Gaussian filter and zero-filled to 16,384 data points. After phase correction at zero and first orders, the baseline of absorption-mode spectrum was corrected. And then, peak heights were used in the quantification of [1-^{13}C] Lac (185 ppm), [1-^{13}C] pyruvate-hydrate (Pyr-Hyd) (181 ppm), [1-^{13}C] Ala (177 ppm), and [1-^{13}C] Pyr (172 ppm). The total carbon (tC) signal was the sum of the peak heights for [1-^{13}C] Lac, [1-^{13}C] Pyr-Hyd, [1-^{13}C] Ala, and [1-^{13}C] Pyr signals. The results were presented as ratios of [1-^{13}C] metabolite signals (Lac/Pyr, Ala/Pyr, Pyr- Hyd/Pyr, Lac/tC, Ala/tC, and Pyr-Hyd/tC).

In addition, C-13 2D metabolic imaging data were apodized with a 9 Hz Gaussian filter, frequency referenced to [1-^{13}C]Pyr, and aligned with anatomic images using Spectroscopic Image Visualization and Computing (SIVIC) software (12). Color-coded heat-maps representing the peak height of hyperpolarized [1-^{13}C]Ala and [1-^{13}C]Lac were generated for the 14 s time point using a sinc-based interpolation of the C-13 2D spectroscopic metabolic imaging data to the resolution of the anatomical images [10, 12]. Also, in order to compare the pattern of metabolic change in dynamic C-13 MRS and 2D spectroscopic metabolic imaging, the levels of hyperpolarized [1-^{13}C]Ala and [1-^{13}C]Lac were measured in the volume of interest (VOI) containing hepatic lesions.

For quantification of the exchange rates, the area under the curve (AUC) ratios of hyperpolarized [1-^{13}C]Lac to [1-^{13}C]Pyr (Lac/Pyr) and [1-^{13}C]Ala to [1-^{13}C]Pyr (Ala/Pyr) were calculated in three groups [13].

The acquired IVIM-DWI data were post-processed on a GE Advance Workstation 4.6 so as to obtain the following parameters: apparent diffusion coefficient (ADC), perfusion fraction (f), true water molecular diffusion coefficient (D), and pseudo-diffusion coefficient (D^*). In this study, the ADC value was calculated by a mono-exponential model based on the following equation: $S_b/S_0 = \exp(-b \times \text{ADC})$, where S_b is the signal intensity in the pixel with diffusion gradient b, and S_0 is the signal intensity in the pixel without a diffusion gradient. IVIM parameters were obtained using a nonlinear bi-exponential fit based on the following equation, according to Le Bihan et al. [14]: $S_b/S_0 = (1 - f) \times \exp(-bD) + f \times \exp[-b(D + D^*)]$. Three regions of interest (ROIs) of ~ 5 mm^2 were manually drawn to avoid the inclusion of vessels/bile ducts and the margin of the liver. For each parameter, the average of measurements from three ROIs was considered as the representative result.

Serum Biochemical Analysis

After acquiring MRS and MRI data, blood samples (0.3– 0.5 ml/mouse) were collected from all mice that had been fasting during 12 h. Serum samples were collected by centrifugation at 3000 rpm for 15 min and stored at − 80 °C until being used for biochemical analyses. Aspartate

aminotransferase (AST), alanine aminotransferase (ALT), lactate dehydrogenase (LDH), creatine kinase (CK), and total protein (TP) were measured by an autoanalyzer using a commercially available test kit (VET TEST 8008; IDEXX Laboratories, Westbrook, ME, USA).

Histopathological Analysis

Liver fragments of approximately $0.5 \times 0.5 \times 0.2$ cm³ were extracted from all mice, and fixed in 10 % formaldehyde. After 24 h of fixation, the fragments were dehydrated, cleared, and embedded in paraffin. Paraffin blocks were cut into 3 μm thick sections and stained by Masson trichrome for the assessment of hepatic fibrosis. The histopathological images were acquired on an IEEE 1394 digital camera (FO124SC; FOculus, Finning, Germany). One pathologist, who was blinded to the information of the mice groups, evaluated the degree of hepatic fibrosis according to the Batts-Ludwig classification system [15]. In this system, scoring is used to evaluate the degree of fibrosis: stage 0, no fibrosis; stage 1, enlarged, fibrotic portal tracts; stage 2, periportal or portal-portal fibrotic septa, but intact architecture; stage 3, septal fibrosis with architectural distortion, but no obvious cirrhosis; and stage 4, probable or definite cirrhosis. Based on the degree of fibrosis, the mice were classified as mild (stages 1 and 2) or severe (stages 3 and 4) fibrosis groups.

Statistical Analysis

The differential metabolite ratios, ADC value, IVIM parameters, and values of serum biochemistry among the three groups were analyzed by a one-way analysis of variance (ANOVA) test and Tukey's post hoc test at $p < 0.05$ using SPSS 19.0 (Chicago, IL, USA). In addition, the correlation of the levels of the [1-^{13}C]metabolites with ADC value and IVIM parameters were analyzed by Spearman's correlation test with a 95 % confidence interval.

Results

Hepatic Histopathology and Serum Biochemistry

Regarding the degree of hepatic fibrosis, 14 mice were categorized as stage 1 ($n = 2$), stage 2 ($n = 5$), stage 3 ($n = 6$), and stage 4 ($n = 1$). Also, the body weights (normal vs. mild vs. severe = 22.64 ± 0.27 g vs. 22.31 ± 0.41 g vs. 21.08 ± 0.47 g), serum AST, ALT, LDH, CK, and TP levels were not significantly different among the three groups at 15-week (Fig. 1).

In vivo C-13 Dynamic MRS and Metabolic Imaging

Figure 2 shows the exemplary spectra reconstructed from the dynamic spectra covering 60 s. The metabolite levels were
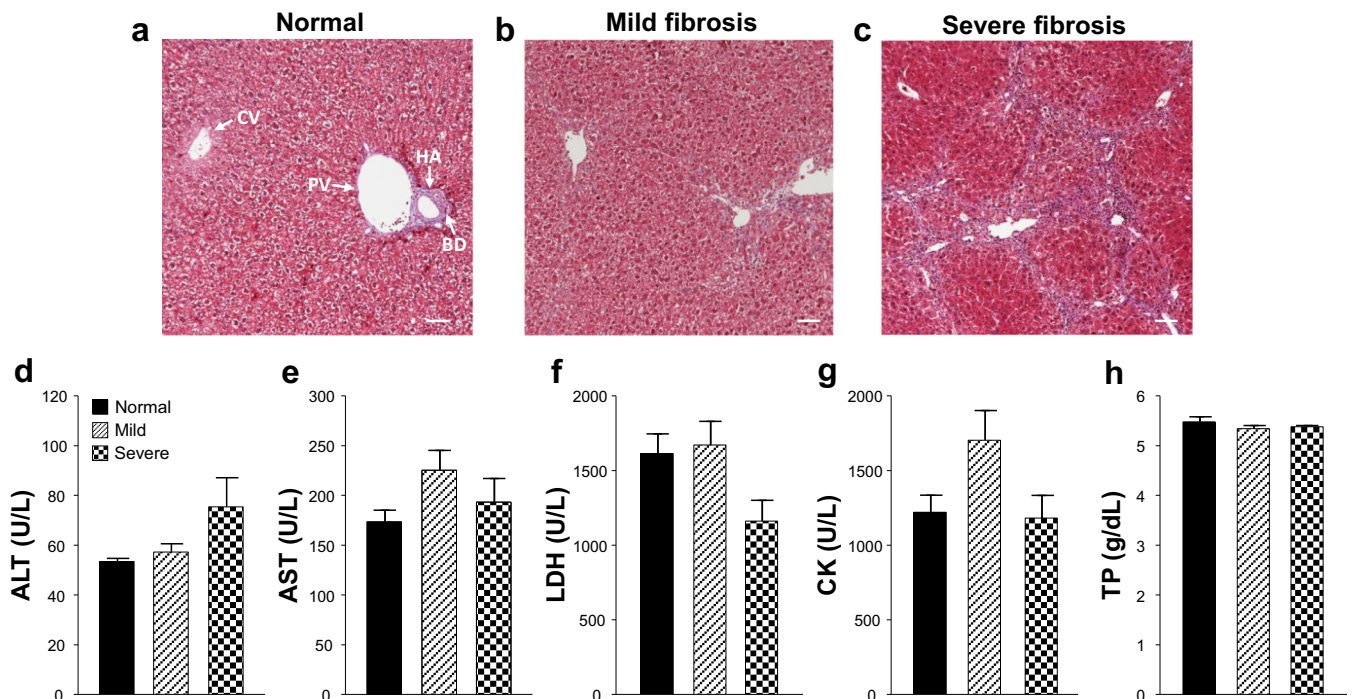

Fig. 1. Histopathology of the hepatic tissue (× 100) in (a) normal (the portal tract shows no fibrosis), (b) mild fibrosis (the portal tracts have irregular fibrous extension), and (c) severe fibrosis (marked fibrous bridges connect the portal tracts. Results of blood chemistry among normal, mild, and severe fibrosis groups (d–h). CV, central vein; PV, portal vein; HA, hepatic artery; BD, bile duct; ALT, alanine aminotransferase; AST, aspartate aminotransferase; LDH, lactate dehydrogenase; CK, creatine kinase; TP, total protein. Bar = 50 μm. Bar graphs represent mean ± standard error of the mean.

significantly different among the three groups. The ratios of [1-^{13}C]Lac/Pyr, [1-^{13}C]Lac/tC, [1-^{13}C]Ala/Pyr, and [1-^{13}C]Ala/tC were significantly higher in both mild and severe fibrosis groups than in the normal control group ($p < 0.05$) (Fig. 3). While the [1-^{13}C]Lac/Pyr and [1-^{13}C]Lac/tC ratios were not significantly different between mild and severe fibrosis groups, the ratios of [1-^{13}C]Ala/Pyr and [1-^{13}C]Ala/tC were significantly higher in the severe fibrosis group than in the mild fibrosis group ($p < 0.05$) (Fig. 3). However, there were no significant differences in the ratios of [1-^{13}C]Pyr-Hyd/Pyr and [1-^{13}C]Pyr-Hyd/tC among the three groups.

Figure 4 displays each C-13 metabolic images for hyperpolarized [1-^{13}C]Lac and [1-^{13}C]Ala signals. The each of metabolic maps showed the differential production of [1-^{13}C]Lac and [1-^{13}C]Ala among the three groups, respectively. In VOI analysis, the ratios of [1-^{13}C]Lac/Pyr (normal *vs.* mild *vs.* severe $= 0.17 \pm 0.02$, 0.63 ± 0.03, and 0.68 ± 0.01, respectively) and [1-^{13}C]Ala/Pyr (0.27 ± 0.01, 0.37 ± 0.03, and 0.55 ± 0.02, respectively) were significantly higher in both mild and severe fibrosis groups than in the normal control group ($p < 0.05$) in line with results of dynamic C-13 MRS.
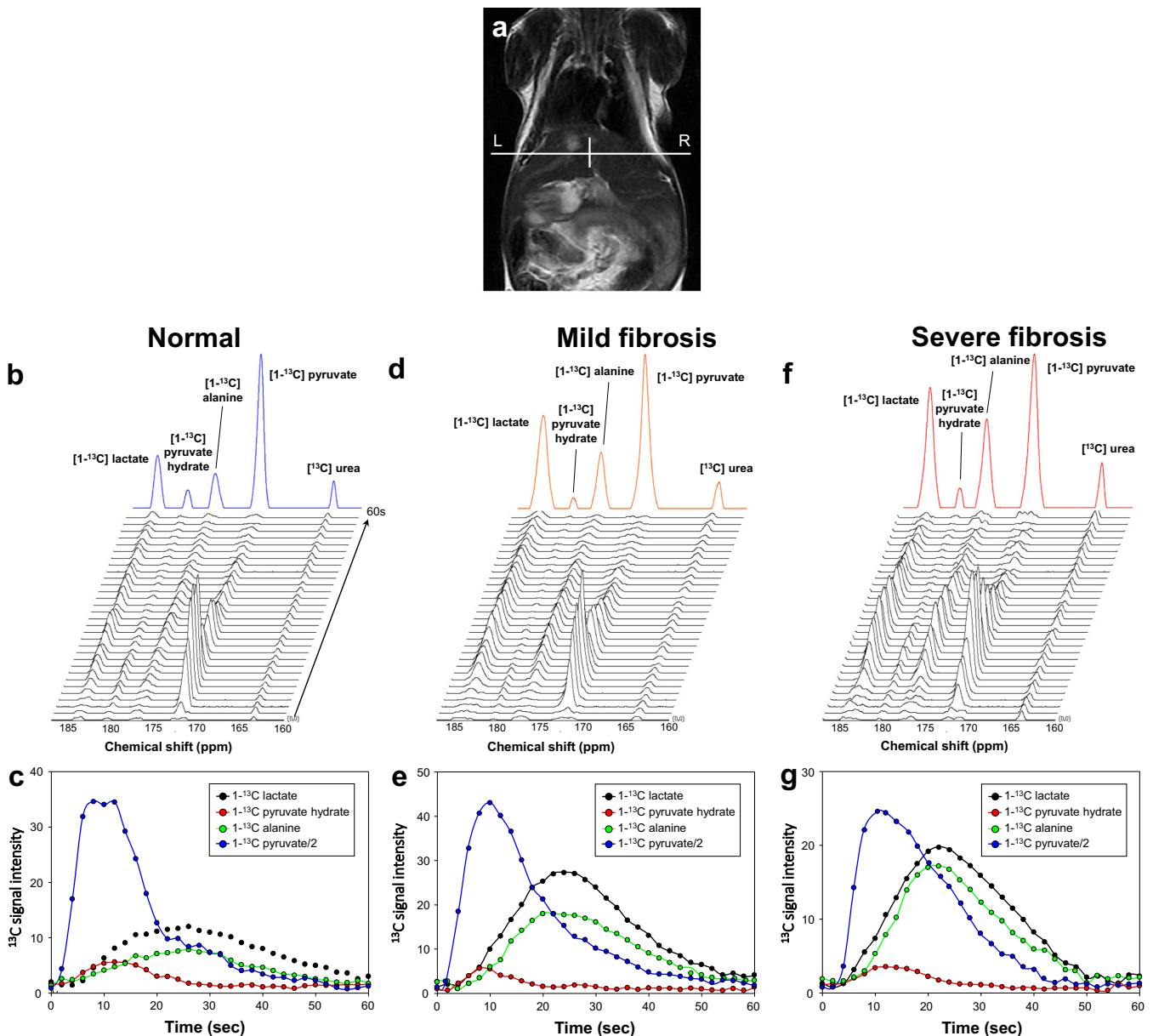

Fig. 2. (a) MRI of mouse. Dynamic C-13 MR spectra of the liver, which were acquired from (b) normal, (d) mild, and (f) severe fibrosis mice. Stacked spectra were acquired every 2 s from a 5.5-mm axial slice of the liver, and signal intensity curves for (c) normal, (e) mild, and (g) severe fibrosis mice demonstrate the time course of conversion of [1-^{13}C] lactate, [1-^{13}C] pyruvate-hydrate, [1-^{13}C] alanine, and [1-^{13}C] pyruvate. The color spectra (b, d, f) represent the sum of the spectra covering a 60-s time span (normal: blue; mild fibrosis: brown; severe fibrosis: red).
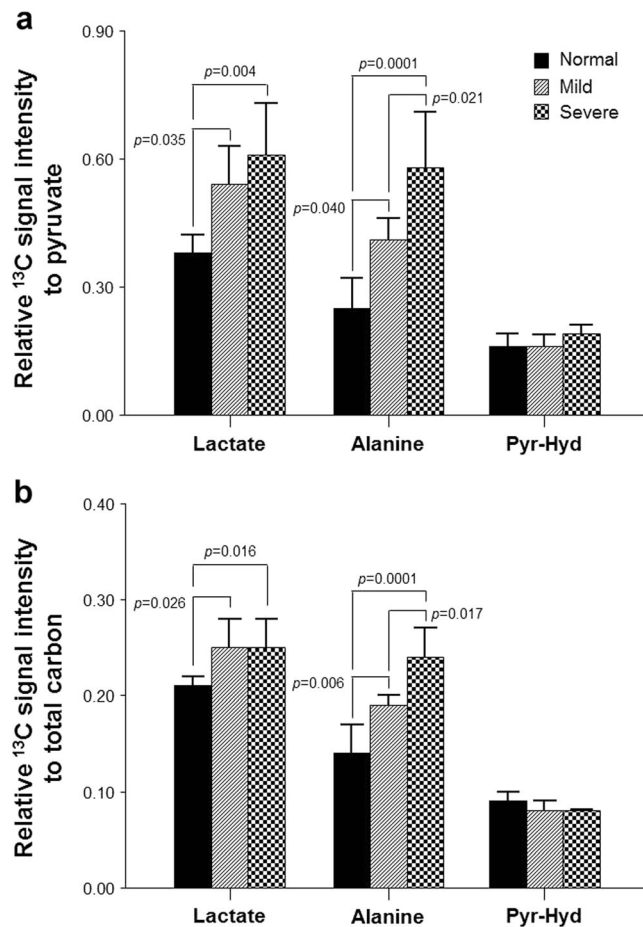
Fig. 3. Cellular metabolite changes in normal, mild, and severe fibrosis groups. The metabolite ratios (a: to pyruvate and b: to total carbon) were significantly different among the three groups ($p < 0.05$). Pyr-Hyd, pyruvate-hydrate. Bar graphs represent mean ± standard deviation.

In addition, the AUC ratios of Lac/Pyr and Ala/Pyr were significantly higher in both mild and severe fibrosis groups than in the normal control group ($p < 0.05$) (Fig. 5).

Comparison of ADC Value and IVIM Parameters

Regarding the ADC value and IVIM parameters, the D^* value was the only significantly different parameter among the three groups ($20.75 \pm 2.06 \times 10^{-3}$ mm^2/s, $15.47 \pm 2.08 \times 10^{-3}$ mm^2/s, and $10.77 \pm 0.81 \times 10^{-3}$ mm^2/s in normal, mild, and sever fibrosis group, respectively) ($p < 0.0001$). However, the values of ADC ($0.82 \pm 0.08 \times 10^{-3}$ mm^2/s, $0.80 \pm 0.09 \times 10^{-3}$ mm^2/s, $0.66 \pm 0.10 \times 10^{-3}$ mm^2/s, respectively), f (29.37 ± 8.41 %, 27.03 ± 3.06 %, 26.03 ± 5.03 %, respectively), and D ($0.38 \pm 0.16 \times 10^{-3}$ mm^2/s, $0.37 \pm 0.15 \times 10^{-3}$ mm^2/s, $0.35 \pm 0.13 \times 10^{-3}$ mm^2/s, respectively) were not significantly different among the three groups.

Correlation of D^* Value with the Levels of the [1-^{13}C]Lac and [1-^{13}C]Ala

The levels of [1-^{13}C]Lac and [1-^{13}C]Ala were negatively correlated with D^* value (Table 1; Fig. 6). However, there were no correlations between [1-^{13}C]metabolite levels and other IVIM parameters among the three groups.

Discussion

Owing to its ability to evaluate pathologic conditions using metabolic changes, hyperpolarized C-13 MRS has been studied for various cardiovascular, neurovascular, and neurological diseases. In particular, our group has applied this technique to abdominal organs [7, 9, 10]. Recently, the use of hyperpolarized [1-^{13}C]substrates to study human diseases is rapidly approaching to the clinic, demonstrating the potential of this technique for staging of prostate cancer [16] and assessment of myocardial metabolism [17]. Therefore, we investigated metabolic alterations in different stages of liver fibrosis using *in vivo* hyperpolarized dynamic C-13 MRS for acquiring high spectral resolution and AUC analysis, as well as 2D metabolic imaging for visualizing hepatic lesions with severity of fibrosis.

In addition to carbon tetrachloride (CCl$_4$) used in a previous study [18], TAA has been widely used to induce animal models of experimental liver fibrosis. Although TAA is not hepatotoxic, the covalent binding of its reactive metabolites to proteins and lipids causes oxidative stress and centrilobular necrosis, as well as leading more periportal infiltrates and pronounced ductal proliferation compared with CCl$_4$ [19]. In this study, we developed mild and severe fibrosis model using C3H/HeN mice with TAA injection based on a previous study [10], demonstrating 0 % mortality in mice and the successful induction of mild and severe fibrosis. Also, our histopathologic findings proved useful to apply TAA-administrated C3H/HeN mouse method for inducing liver fibrosis. Thus, the experimental results in this study can be more related to actual fibrosis severity/progression studies conducted in humans.

Although previous studies [7, 9, 10] have suggested that liver dysfunction was associated with the conversion rate of [1-^{13}C]Pyr to [1-^{13}C]Lac and [1-^{13}C]Ala in biochemical pathways, cellular metabolite changes in various stages of liver fibrosis have not yet been identified. Our study demonstrated that levels of [1-^{13}C]Lac and [1-^{13}C]Ala were elevated in both mild and severe fibrosis groups compared to normal control group. This may be potentially due to the alteration of glycolysis and gluconeogenesis in hepatic metabolism, which could result in the increase in Lac and Ala levels in conjunction with hepatic fibrogenesis. Furthermore, AUC ratios of Lac-Pyr and Ala-Pyr were significantly different among the three groups. Hyperpolarized dynamic data enabled us to perform AUC analysis in terms of exchange rates, which produces similar statistical results to kinetic modeling described by Daniels et al. [13].
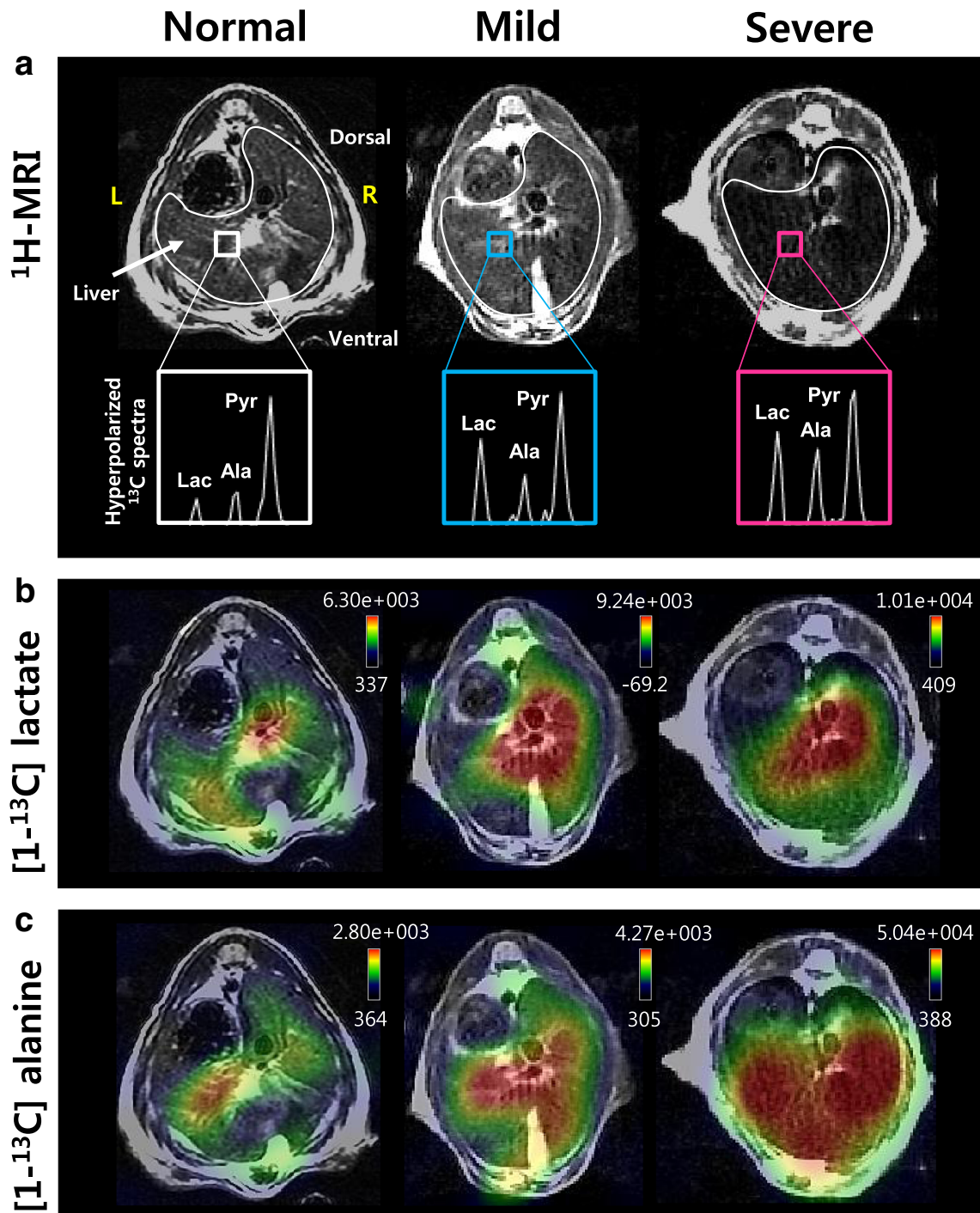
Fig. 4. (a) Representative ^{13}C-13 2D spectroscopic metabolic images. Representative anatomical images, hyperpolarized ^{13}C spectra from the volume of interest (VOI), and metabolic images of (b) [1-^{13}C] lactate and (c) [1-^{13}C] alanine in normal control (left), mild (middle), and severe (right) fibrosis mice. R, right; L, left.

Ala plays a crucial role in amino acid uptake and catabolism in the hepatocytes following reaction [20]: alanine + 0.5 NAD$^+$ + 0.05 NADP$^+$ + H$_2$O $\leftrightarrow$ pyruvate + NH$_4^+$ + 0.5 NADH + 0.5 NADPH + H$^+$. In other words, Ala is an important carrier of nitrogen and carbon during protein degradation, as well as being a highly gluconeogenic amino acid [7]. From these findings mentioned above, our results support the assumption that increased conversion of [1-^{13}C]Pyr to [1-^{13}C]Ala may be related

to the fibrosis-caused disruptions to transamination in metabolic fluxes in hepatic cells. According to a previous study [9], in an acute hepatocyte injury model of chemical-induced hepatotoxicity, the Ala/tC ratio was significantly increased, as compared to those in normal liver. Our results are also in agreement of Kim's study. Thus, it seems that the Ala peak can be a noninvasive and sensitive biomarker for liver diseases with a variety of histopathological states. In addition, Ansley et al. [21] found
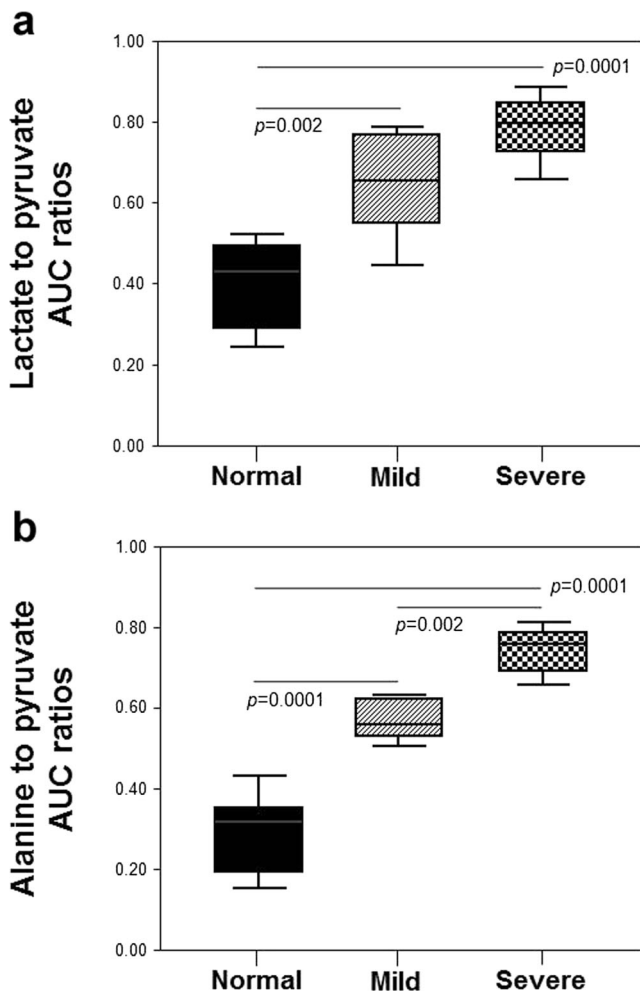
Fig. 5. The AUC ratios of (a) lactate/pyruvate and (b) alanine/pyruvate in normal, mild, and severe fibrosis mice. The AUC ratios were significantly different among the three groups ($p < 0.05$).

and severe fibrosis groups compared to the normal control group. Lac is a major precursor for gluconeogenesis [23]. More importantly, under anaerobic conditions, Pyr is converted to Lac by LDH according to the following reaction: pyruvate + NADH + H$^+$ ⇆ lactate + NAD$^+$ [10]. It has been suggested that the [1-^{13}C]Lac/[1-^{13}C] Pyr ratio in intact cells is a robust indicator of the free cytosolic [NAD$^+$]/[NADH] ratio, which reflects metabolic alterations leading to, or correlating with, pathological states [24]. The liver is recognized as an important organ of acid-base regulation, playing a crucial role in various homeostatic pathways such as the metabolism of organic acid anions including Lac and amino acids [25]. While the healthy liver has a huge functional reservoir of metabolizing Lac, this Lac clearance is impaired in chronic liver diseases because of a decrease in the functional hepatocyte mass [25]. Bihari et al. [26] reported that the elevated Lac levels in patients with liver disease resulted from defects in hepatic Pyr metabolism with a reduction in hepatic gluconeogenesis following severe hepatic dysfunction. Moreover, a clinical study [27] using physical and chemical parameters suggested that lactic acidosis in patients with cirrhosis resulted from both increased Lac production and decreased hepatic Lac disposal. Therefore, [1-^{13}C]Lac is implicated as an important indicator of the progression of hepatic fibrosis and pathophysiology, suggesting that the [1-^{13}C]Lac level might be a noninvasive metabolic biomarker for the diagnosis of liver fibrosis.

In our study, D^*, which represents the perfusion-related parameter, showed a significantly lower value in the severe fibrosis group than in the normal or mild fibrosis groups, but there were no significant differences in ADC, f, and D values among the three groups. More importantly, the value of D^* negatively correlated with the levels of [1-^{13}C]Lac and [1-^{13}C]Ala. It is widely accepted that liver fibrosis is associated with reduced hepatic perfusion and the increased arterial flow triggered by intrahepatic portal hypertension in liver fibrosis is insufficient to compensate for the reduced portal flow [28]. Lu et al. [29] revealed that D^* was significantly lower in patients with liver fibrosis than in healthy subjects, suggesting that decreased D^* in the liver might be associated with the severity of fibrosis. Our results demonstrated that decreased blood perfusion after liver fibrosis might be closely correlated with hepatic metabolism of Lac and Ala. From these findings, the levels of hyperpolarized C-13 metabolites in conjunction with D^* could

that the Ala concentration in the blood may be increased in severe liver disease. Elia et al. [22] also reported that the ability to remove an Ala serum load was significantly decreased in patients with liver cirrhosis, suggesting that Ala should be regarded as an important amino acid in the evaluation of hepatopathy. Therefore, our findings suggest that [1-^{13}C]Ala level in hepatic parenchyma can be potentially considered as a quantitative biomarker for the early diagnosis and staging of liver fibrosis.

Our study also showed that [1-^{13}C]Lac/Pyr and [1-^{13}C]Lac/tC ratios were significantly increased in both mild

Table 1.. Correlations of ADC, f, D, and D^* values with the levels of the [1-^{13}C]lactate and [1-^{13}C]alanine

	ADC		f		D		D^*	
	Coefficients	p values	Coefficients	p values	Coefficients	p values	Coefficients	p values
Lactate/pyruvate	− 0.243	0.382	0.149	0.597	− 0.206	0.462	− 0.706	0.004
Alanine/pyruvate	0.357	0.191	− 0.052	0.854	− 0.277	0.318	− 0.830	0.001
Lactate/total carbon	− 0.312	0.258	0.238	0.392	− 0.083	0.768	− 0.568	0.007
Alanine/total carbon	− 0.312	0.258	− 0.147	0.601	− 0.319	0.247	− 0.847	0.001
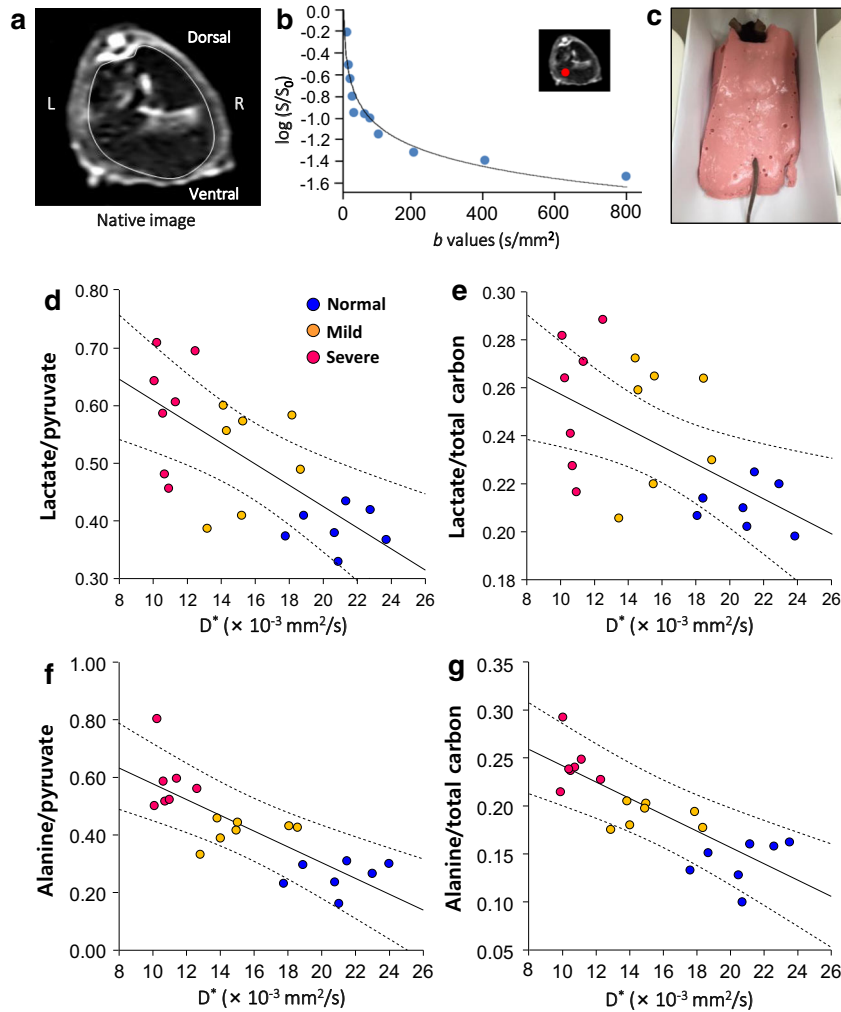
Fig. 6. A correlation between D^* value and the levels of the [1-^{13}C] lactate and [1-^{13}C] alanine. (a) Representative native image obtained with b value of 60 s/mm^2. (b) Logarithmic plot of bi-exponential signal decay from a single pixel (red dot in the inserted image) as a function of 쀸 values on the liver. (c) The solid alginate-mouse chamber was made after liquid alginate was poured around the mouse. A correlation between D^* value and (d) [1-^{13}C] lactate/pyruvate ($\gamma = -0.706$, $p = 0.004$), (e) [1-^{13}C] lactate/tC ($\gamma = -0.568$, $p = 0.007$), (f) [1-^{13}C] alanine/pyruvate ($\gamma = -0.830$, $p = 0.001$), and (g) [1-^{13}C] alanine/tC ($\gamma = -0.847$, $p = 0.001$) is statistically significant in the three groups, where the band with dotted lines shows 95 % confidence intervals.

provide clinically useful information for early detection and staging of liver fibrosis, as well as altered liver parenchymal perfusion. However, further follow-up studies may be needed to conceptually explain the relationship between [1-^{13}C]pyruvate metabolic changes and D^* at different stages of fibrotic evolution with the help of physiological and biochemical analyses, as well as to provide potential options for effective treatment of hepatic fibrosis.

The present study demonstrates for the first time that the cellular metabolite changes of [1-^{13}C]Ala and [1-^{13}C]Lac and their correlation with IVIM parameters could be associated with the hepatic fibrosis. However, our study includes some limitations. Firstly, the sample size was small. Given the limited sample size, future longitudinal studies involving more mice are needed to validate changes in [1-^{13}C]Pyr metabolism and IVIM-DWI in the experimental model of liver fibrosis. Secondly, mild and severe fibrosis models using C3H/HeN mice were induced by TAA injection. Future studies are needed to validate whether our results could also be applicable

to other types of liver fibrosis. Thirdly, in this study, although we additionally used 10 % ethanol-containing water per-oral, we have focused on the development of liver fibrosis induced by TAA injection. Given that there would be a possible metabolic effect of the ethanol in the liver, a further study might be needed to assess the effect of 10 % ethanol on *in vivo* metabolic changes in the liver. Fourthly, for IVIM-DWI, although we used the solid alginate-mouse chamber in order to solve the problems such as motion artifacts [10], the spatial resolution was low for a mouse. Also, the slice thickness was roughly one third of the thickness of the liver. Thus, there would be a concern regarding partial volume effect. This could limit the translatability of our findings to human studies.

Conclusions

Our findings demonstrated that it might be possible to differentiate mild from severe liver fibrosis using the cellular

metabolic changes with hyperpolarized ^{13}C MRS and metabolic imaging.

Compliance with Ethical Standards

Conflict of Interest

The authors declare that they have no conflict of interest.

Publisher's Note. Springer Nature remains neutral with regard to jurisdictional claims in published maps and institutional affiliations.

References

1. Faria SC, Ganesan K, Mwangi I, Shiehmorteza M, Viamonte B, Mazhar S, Peterson M, Kono Y, Santillan C, Casola G, Sirlin CB (2009) MR imaging of liver fibrosis: current state of the art. Radiographics 29:1615–1635

2. Ebrahimi H, Naderian M, Sohrabpour AA (2016) New concepts on pathogenesis and diagnosis of liver fibrosis; a review article. Middle East J Dig Dis 8:166–178

3. Manning DS, Afdhal NH (2008) Diagnosis and quantitation of fibrosis. Gastroenterology 134:1670–1681

4. Harada TL, Saito K, Araki Y, Matsubayashi J, Nagao T, Sugimoto K, Tokuuye K (2018) Prediction of high-stage liver fibrosis using ADC value on diffusion-weighted imaging and quantitative enhancement ratio at the hepatobiliary phase of Gd-EOB-DTPA-enhanced MRI at 1.5 T. Acta Radiol 59(5):509–516

5. Petitclerc L, Sebastiani G, Gilbert G, Cloutier G, Tang A (2017) Liver fibrosis: review of current imaging and MRI quantification techniques. J Magn Reson Imaging 45:1276–1295

6. Lurie Y, Webb M, Cytter-Kuint R, Shteingart S, Lederkremer GZ (2015) Non-invasive diagnosis of liver fibrosis and cirrhosis. World J Gastroenterol 21:11567–11583

7. Moon CM, Oh CH, Ahn KY, Yang JS, Kim JY, Shin SS, Lim HS, Heo SH, Seon HJ, Kim JW, Jeong GW (2017) Metabolic biomarkers for non-alcoholic fatty liver disease induced by high-fat diet: in vivo magnetic resonance spectroscopy of hyperpolarized [1-^{13}C]pyruvate. Biochem Biophys Res Commun 482:112–119

8. Spielman DM, Mayer D, Yen YF, Tropp J, Hurd RE, Pfefferbaum A (2009) In vivo measurement of ethanol metabolism in the rat liver using magnetic resonance spectroscopy of hyperpolarized [1-^{13}C]pyruvate. Magn Reson Med 62:307–313

9. Kim GW, Oh CH, Kim JC, Yoon W, Jeong YY, Kim YH, Kim JK, Park JG, Kang HK, Jeong GW (2016) Noninvasive biomarkers for acute hepatotoxicity induced by 1,3-dichloro-2-propanol: hyperpolarized ^{13}C dynamic MR spectroscopy. Magn Reson Imaging 34:159–165

10. Moon CM, Shin SS, Lim NY, Kim SK, Kang YJ, Kim HO, Lee SJ, Beak BH, Kim YH, Jeong GW (2018) Metabolic alterations in a rat model of hepatic ischemia reperfusion injury: in vivo hyperpolarized ^{13}C MRS and metabolic imaging. Liver Int 38(6):1117–1127

11. Thomas RG, Moon MJ, Kim JH, Lee JH, Jeong YY (2015) Effectiveness of losartan-loaded hyaluronic acid (HA) micelles for the reduction of advanced hepatic fibrosis in C3H/HeN mice model. PLoS One 10:e0145512

12. Crane JC, Olson MP, Nelson SJ (2013) SIVIC: open-source, standards-based software for DICOM MR spectroscopy workflows. Int J Biomed Imaging 2013:169526

13. Daniels CJ, McLean MA, Schulte RF et al (2016) A comparison of quantitative methods for clinical imaging with hyperpolarized (13)C-pyruvate. NMR Biomed 29(4):387–399

14. Le Bihan D, Breton E, Lallemand D (1988) Perfusion in intravoxel incoherent motion MR imaging. Radiology 168:497–505

15. Batts KP, Ludwig J (1995) Chronic hepatitis: an update on terminology and reporting. Am J Surg Pathol 19:1409–1417

16. Nelson SJ, Kurhanewicz J, Vigneron DB, Larson PEZ, Harzstark AL, Ferrone M, van Criekinge M, Chang JW, Bok R, Park I, Reed G, Carvajal L, Small EJ, Munster P, Weinberg VK, Ardenkjaer-Larsen JH, Chen AP, Hurd RE, Odegardstuen LI, Robb FJ, Tropp J, Murray JA (2013) Metabolic imaging of patients with prostate cancer using hyperpolarized [1-^{13}C] pyruvate. Sci Transl Med 5:198ra108

17. Cunningham CH, Lau JY, Chen AP et al (2016) Hyperpolarized ^{13}C metabolic MRI of the human heart: initial experience. Circ Res 119(11):1177–1182

18. Josan S, Billingsley K, Orduna J, Park JM, Luong R, Yu L, Hurd R, Pfefferbaum A, Spielman D, Mayer D (2015) Assessing inflammatory liver injury in an acute CCl$_4$ model using dynamic 3D metabolic imaging of hyperpolarized [1-(13)C] pyruvate. NMR Biomed 28(12):1671–1677

19. Wallace MC, Hamesch K, Lunova M, Kim Y, Weiskirchen R, Strnad P, Friedman SL (2015) Standard operating procedures in experimental liver research: thioacetamide model in mice and rats. Lab Anim 49:21–29

20. Chan C, Berthiaume F, Lee K et al (2003) Metabolic flux analysis of cultured hepatocytes exposed to plasma. Biotechnol Bioeng 81(1):33–49

21. Ansley JD, Isaacs JW, Rikkers LF, Kutner MH, Nordlinger BM, Rudman D (1978) Quantitative tests of nitrogen metabolism in cirrhosis: relation to other manifestations of liver disease. Gastroenterology 75:570–579

22. Elia M, Ilic V, Bacon S, Williamson DH, Smith R (1980) Relationship between the basal blood alanine concentration and the removal of an alanine load in various clinical states in man. Clin Sci (Lond) 58:301–309

23. Xie B, Waters MJ, Schirra HJ (2012) Investigating potential mechanisms of obesity by metabolomics. J Biomed Biotechnol 2012:805683

24. Christensen CE, Karlsson M, Winther JR, Jensen PR, Lerche MH (2014) Non-invasive in-cell determination of free cytosolic [NAD$^+$]/[NADH] ratios using hyperpolarized glucose show large variations in metabolic phenotypes. J Biol Chem 289:2344–2352

25. Mazzeo AT, Maimone S (2018) Acid-base disorders in liver disease. J Hepatol 68(3):617–618

26. Bihari D, Gimson AE, Lindridge J, Williams R (1985) Lactic acidosis in fulminant hepatic failure. Some aspects of pathogenesis and prognosis. J Hepatol 1:405–416

27. Funk GC, Doberer D, Kneidinger N, Lindner G, Holzinger U, Schneeweiss B (2007) Acid-base disturbances in critically ill patients with cirrhosis. Liver Int 27:901–909

28. Zhang B, Liang L, Dong Y, Lian Z, Chen W, Liang C, Zhang S (2016) Intravoxel incoherent motion MR imaging for staging of hepatic fibrosis. PLoS One 11:e0147789

29. Lu PX, Huang H, Yuan J, Zhao F, Chen ZY, Zhang Q, Ahuja AT, Zhou BP, Wáng YXJ (2014) Decreases in molecular diffusion, perfusion fraction and perfusion-related diffusion in fibrotic livers: a prospective clinical intravoxel incoherent motion MR imaging study. PLoS One 9:e113846